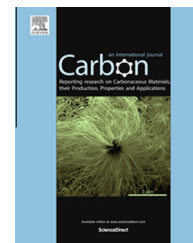


Available at [www.sciencedirect.com](http://www.sciencedirect.com)

ScienceDirect

journal homepage: [www.elsevier.com/locate/carbon](http://www.elsevier.com/locate/carbon)

# High sensitivity surface enhanced Raman spectroscopy of R6G on *in situ* fabricated Au nanoparticle/graphene plasmonic substrates



Rongtao Lu <sup>a,\*</sup>, Annika Konzelmann <sup>a</sup>, Feng Xu <sup>b</sup>, Youpin Gong <sup>a</sup>, Jianwei Liu <sup>a</sup>, Qingfeng Liu <sup>a</sup>, Melisa Xin <sup>a</sup>, Rongqing Hui <sup>b</sup>, Judy Z. Wu <sup>a,\*</sup>

<sup>a</sup> Department of Physics & Astronomy, University of Kansas, Lawrence, KS 66045, USA

<sup>b</sup> Department of Electrical Engineering & Computer Science, University of Kansas, Lawrence, KS 66045, USA

## ARTICLE INFO

### Article history:

Received 16 September 2014

Accepted 16 January 2015

Available online 22 January 2015

## ABSTRACT

Plasmonic gold nanoparticles (AuNP) with controllable dimensions have been fabricated *in situ* on graphene at moderately elevated temperature for high sensitivity surface enhanced Raman spectroscopy (SERS) of Rhodamine 6G (R6G) dye molecules. Significantly enhanced Raman signature of R6G dyes were observed on AuNP/graphene substrates as compared to the case without graphene with an improvement factor of 400%, which is remarkably greater than previous results obtained in *ex situ* fabricated SERS substrate. Simulation of localized electromagnetic field around AuNPs with and without the underneath graphene layer reveals an enhanced local electromagnetic field due to the plasmonic effect of AuNPs, while additional Ohmic loss occurs when graphene is present. The enhanced local electromagnetic field by plasmonic AuNPs is unlikely the dominant factor contributing to the observed high SERS sensitivity on R6G/AuNP/graphene substrate. Instead, the p-doped graphene, which is supported by the large positive Dirac point shift away from “zero” observed in AuNP/graphene field effect transistors, promotes SERS signals through enhanced molecule adsorption and non-resonance molecular–substrate chemical interaction.

© 2015 Elsevier Ltd. All rights reserved.

## 1. Introduction

Surface enhanced Raman spectroscopy (SERS) provides high sensitivity and selectivity on molecule detection [1,2]. SERS substrates play a critical role in facilitating molecule adsorption and optimizing SERS sensitivity through both electromagnetic and chemical mechanisms [3]. Recently, graphene has become a promising SERS substrate material with appropriate chemical inertness and compatibility to biological species [3,4]. Graphene was first reported as a substrate to

suppress fluorescence interference in Raman measurements [5]. This prompted further exploration as well as demonstration of SERS on some commonly used Raman probe dyes on graphene [4] and plasmonic metal nanoparticle/graphene substrates [6]. In the nanoparticle/graphene SERS substrates, electromagnetic mechanism was previously reported as the dominant contribution to the enhanced SERS sensitivity because of the remarkably enhanced electromagnetic field in proximity of the metal nanoparticles due to the localized surface plasmonic resonance (LSPR) of electrons on these

\* Corresponding authors: Fax: +1 785 864 5262.

E-mail addresses: [rtlu@ku.edu](mailto:rtlu@ku.edu) (R. Lu), [jwu@ku.edu](mailto:jwu@ku.edu) (J.Z. Wu).

<http://dx.doi.org/10.1016/j.carbon.2015.01.028>

0008-6223/© 2015 Elsevier Ltd. All rights reserved.

nanoparticles [3]. However, more complicated chemical mechanism also coexists and may enhance Raman scattering by varying the coupling between molecule species and the graphene substrate via changing the molecule–graphene distance, molecular orientation, and electronic energy level of graphene and species, etc. [3,6]. Understanding the electromagnetic and chemical mechanisms in SERS sensitivity at microscopic scales is important for development of high sensitivity metal nanoparticle/graphene SERS substrates.

It should be realized that the SERS effect is strongly affected by the morphology of metal nanoparticles and their interface with graphene. Flat substrate geometry has advantages in obtaining controllable configuration and morphology of the metal nanoparticle/graphene substrates [3,6,7]. Since the enhanced electromagnetic field locates primarily around the plasmonic metal nanoparticles, an optimal SERS substrate needs to have an effective inter-particle gap coverage while maintaining the gap width on the order of a few nanometers. This requires controlling the metal nanoparticle dimension small while compromising LSPR Ohmic loss [8]. In previous reports, lithographic patterning [7] and fabrication of self-assembled metal (Au or Ag) islands were reported on CVD (chemical vapor deposition) graphene sheets with considerably enhanced molecule SERS sensitivity [6]. The former requires complicated lithographic procedures and the residues of photoresist and other chemicals used could have detrimental effects to the SERS sensitivity by degrading both electromagnetic and chemical SERS enhancement factors. In the latter, an *ex situ* procedure was employed in which graphene and metal islands are exposed to multiple chemicals for graphene transfer and cleaning, and the method only provides limited control over the metal islands morphology. Attempt to fabricate metal nanoparticles on graphene using chemical method for DNA SERS may provide a low-cost approach while nanoparticle density, especially achieving high densities for optical gap size and coverage between nanoparticles, remains a challenge [9]. Alternatively, doping graphene has been reported to moderately enhance Raman scattering, which is interesting if such an effect could be combined with plasmonic effect from the metal nanoparticle decoration [10]. This motivates us to explore controllable *in situ* self-assembly of Au nanoparticles (AuNPs) on pre-cleaned CVD graphene transferred on glass or SiO<sub>2</sub>/Si substrates, as illustrated in Fig. 1. By selecting appropriate substrate

temperatures and Au thickness during high-vacuum deposition, the dimension of the AuNPs can be systematically varied and the inter-AuNP gap coverage up to 69.6% has been obtained. The unique advantage of this approach is in eliminating chemical contamination during the entire AuNP/graphene substrate fabrication and in achieving controllable AuNP morphology on graphene in a scalable fashion. In this paper, we report experimental results of *in situ* fabrication of plasmonic AuNP/graphene substrates and investigation, using both computational simulation and experimental characterization, of the SERS sensitivity of Rhodamine 6G (R6G) using these substrates. Significantly enhanced Raman signature of R6G dyes were observed on these AuNP/graphene substrates as compared to the case without graphene with an improvement factor of 400%, which represents a remarkable improvement over the previous results obtained using *ex situ* fabricated SERS substrates.

## 2. Experimental

Single layer CVD graphene sheets were transferred onto Si (100) substrates with 90 nm thermal oxide [11,12]. A thin layer of polymethylmethacrylate (PMMA) was spun on top of graphene, and the Cu sheet under graphene was removed using CE-100 copper etchant prior to transfer. After transfer, the samples were thoroughly cleaned in acetone for multiple times, followed with annealing in mixed Ar/H<sub>2</sub> gas (1:1, 500 sccm each) at 400 °C for 1 h to remove residues of PMMA and other chemicals. AuNPs were electron-beam evaporated [13] on the heated graphene/SiO<sub>2</sub>/Si samples in high vacuum of  $<5 \times 10^{-6}$  Torr. Considering the eutectic temperature between Au and Si is around 346 °C, slightly higher substrate temperatures are usually selected to form circular shaped AuNPs on SiO<sub>2</sub> or similar surfaces [14,15]. However, since high temperatures may cause graphene degradation via reaction with residue gases such as oxygen in the vacuum chamber, lower substrate temperatures are preferred. In this work, we have found AuNPs can be well formed *in situ* during Au evaporation at moderate temperatures of 250–300 °C. At these temperatures, graphene remain intact based on Raman analysis and electrical transport measurement (to be discussed later). In order to obtain AuNPs with variable dimensions, the nominal film thickness of the evaporated Au was selected at 2, 4, 8 and 12 nm, respectively. Several sets of samples were fabricated for consistency. The sample surface morphology was characterized using a LEO 1550 field emission scanning electron microscopy (SEM) system, and the SEM images were analyzed using an image analysis software ImageJ (National Institutes of Health, Bethesda, MD) [16] to quantify the inter-particle gap coverage. Optical transmittance measurements were carried out on AuNP/glass samples using a Horiba iHR550 spectrometer and an integration sphere. Raman spectroscopy was performed using a WiTec Alpha 300 system with a 633 nm laser (5 mW for AuNP/graphene samples) and a 100× objective. Before SERS measurements, samples were immersed into 50 μM Rhodamine 6G (R6G; R4127-5G, Sigma-Aldrich) solution for overnight, which was followed with rinse of methanol and baking at 150 °C for 1 h. All SERS measurement conditions were kept the same with the laser power at

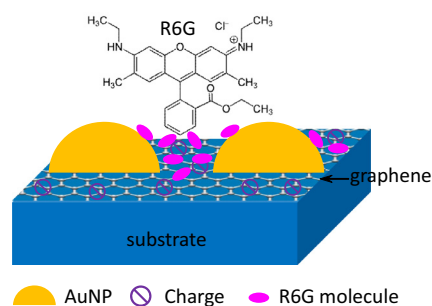


**Fig. 1** – Diagram of R6G molecules attached on AuNP/graphene SERS substrate. Molecular structure of R6G is illustrated. (A color version of this figure can be viewed online.)

a low level of approximately 1 mW to avoid damage of the R6G molecules. Graphene field effect transistors (GFETs) with a channel area of  $20 \times 20 \mu\text{m}^2$  were fabricated on  $\text{SiO}_2$  (90 nm)/Si by following the procedures reported earlier and AuNPs were deposited onto the GFET channel through a shadow mask [17]. Transport properties of the GFETs with and without AuNPs were measured both in air and high vacuum in a home-made probe station system.

### 3. Results and discussion

Fig. 2 shows the SEM images of AuNPs fabricated on  $\text{SiO}_2$ /Si substrates [AuNP/ $\text{SiO}_2$ /Si, (a)–(d)] and graphene/ $\text{SiO}_2$ /Si [AuNP/graphene, (e)–(h)], respectively, with different nominal gold film thicknesses of 2 nm [(a) and (e)], 4 nm [(b) and (f)], 8 nm [(c) and (g)] and 12 nm [(d) and (h)]. A variation trend of monotonically increasing AuNP dimension, defined as the longest distance between any two points along the particle boundary and also called Feret's diameter [16], with the nominal film thickness is clearly shown on both types of substrates. As summarized in Table 1, the mean dimension of AuNP is about 14.3 nm for Au nominal thickness of 2 nm, which increases to 43.8 nm at 12 nm thickness on the  $\text{SiO}_2$ /Si substrate. Interestingly, comparable dimensions were observed on AuNPs on graphene/ $\text{SiO}_2$ /Si and  $\text{SiO}_2$ /Si substrates, respectively, at the same nominal Au film thickness (Table 1). The irregular shape of the AuNPs on both kinds of

substrates may be attributed to the lower substrate temperature employed for Au evaporation [14,18]. While the AuNPs become more circular in shape and larger in dimension at higher substrate temperatures due to high mobility of Au atoms on the substrate [18,19], lower temperatures were selected in this work to avoid degradation of graphene. The AuNP area coverage percentage increases monotonically with nominal Au film thickness for both sets of samples shown in Fig. 2. This means the inter-AuNP gap coverage area percentage increases monotonically with decreasing AuNP dimension and reaches a maximum of 69.6% at the smallest nominal Au thickness of 2 nm, which is considerably higher than the Au island case fabricated at room temperature [6], at a comparable Au thickness. Considering the enhanced electromagnetic fields localize around the plasmonic AuNPs, the increased gap coverage is advantageous to high SERS sensitivity.

The LSPR of the AuNPs is clearly illustrated in the optical transmittance spectra of AuNP/graphene/glass as well as AuNP/glass samples as shown in Fig. 3. The LSPR wavelength  $\lambda_p$  and the minimum transmittance at  $\lambda_p$  are summarized in Table 1 and categorized in corresponding rows of AuNP/ $\text{SiO}_2$  and AuNP/graphene, respectively. Basically, in both cases of either with or without graphene the  $\lambda_p$  red shifts to longer wavelength with increasing AuNP dimension, which is consistent with previous works [12,13] and is also confirmed as result of the NP dimension effect for plasmonic resonance,

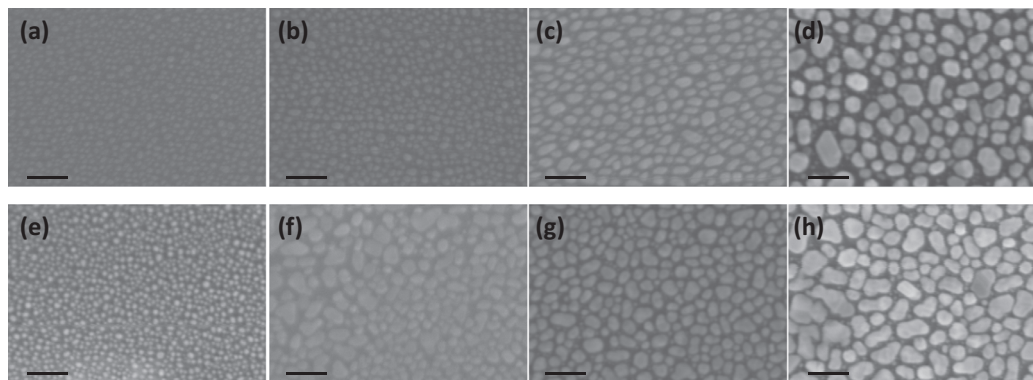
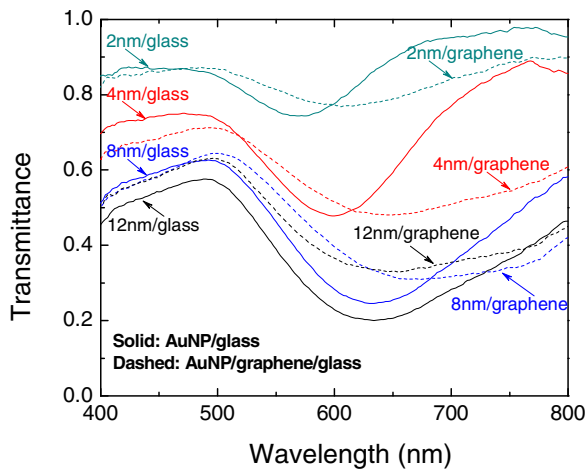


Fig. 2 – Surface morphologies of in-situ fabricated Au NP on  $\text{SiO}_2$ /Si [(a)–(d)] and CVD graphene [(e)–(h)] with different nominal Au thicknesses of: 2 nm [(a) and (e)], 4 nm [(b) and (f)], 8 nm [(c) and (g)] and 12 nm [(d) and (h)]. Scale bar is 100 nm.

Table 1 – Dimension and optical properties of AuNP on bare substrate and graphene.

	Mean dimension (nm) [ $\pm$ standard deviation (nm)]	AuNP area coverage (%)	LSPR wavelength $\lambda_p$ (nm)	Minimum transmittance at $\lambda_p$ (%)	Mean gap width (nm) [ $\pm$ standard deviation (nm)]
2 nm AuNP/ $\text{SiO}_2$	14.3 $\pm$ 7.4	32.8	570	74.4	–
4 nm AuNP/ $\text{SiO}_2$	20.1 $\pm$ 11.9	44.6	598	47.8	–
8 nm AuNP/ $\text{SiO}_2$	32.4 $\pm$ 14.9	50.3	632	24.5	–
12 nm AuNP/ $\text{SiO}_2$	43.8 $\pm$ 19.0	52.3	634	20.0	–
2 nm AuNP/graphene	13.6 $\pm$ 7.2	30.4	606	76.8	6.99 $\pm$ 2.51
4 nm AuNP/graphene	31.5 $\pm$ 16.1	45.8	648	48.1	9.03 $\pm$ 3.70
8 nm AuNP/graphene	31.2 $\pm$ 12.9	55.0	666	31.0	7.39 $\pm$ 3.24
12 nm AuNP/graphene	46.2 $\pm$ 26.4	64.2	654	33.0	8.96 $\pm$ 2.84



**Fig. 3 – Optical transmittance spectra of AuNP/glass (solid) and AuNP/graphene/glass (dashed). (A color version of this figure can be viewed online.)**

as indicated later in Fig. 4. In addition, the spectra of the AuNP/graphene/glass samples show a clear red-shift and transmittance reduction and hence broadened full width at half maximum (FWHM) of the resonance peaks as compared to their counterparts' in absence of graphene, which is a clear sign of the graphene layer induced additional Ohmic loss and consequently lower quality factor [12].

To quantify the damping effect of the graphene on AuNP/graphene substrates, we have performed finite-difference time-domain (FDTD) simulation based on FULLWAVE simulation package [20]. The simulation employed two ideal Au hemispheres on the front surface of a semi-infinite  $\text{SiO}_2$  substrate, and a single layer of graphene was placed in between the AuNPs and  $\text{SiO}_2$  substrate. A plane lightwave was launched in the surface normal direction ( $z$ -direction) with a single polarized electrical field  $E_x$ . Although the shape of the AuNPs shown in Fig. 2 is largely irregular, strong field

concentration due to plasmonic effect is often localized near sharp edges of metal particles, thus we use two relatively small Au hemispheres of 7 nm in diameter in the simulation to model the interaction between them as the gap size is varied. The simulation was performed in a  $30 \times 30 \times 30 \text{ nm}^3$  space centered at the middle point between the two Au hemispheres. Perfectly matched layer (PML) conduction was used for the boundary of simulation window which absorbs the energy without inducing reflections. The gap between the two Au hemispheres was varied in the simulation to demonstrate the impact of the interference between them.

To investigate the LSPR effect of plasmonic metal NPs, optical power flow was integrated over a box surrounding the Au hemispheres using the Q-calculation function of the simulation package, and the calculated quality factor  $Q$  value is proportional to the absorption cross section of the AuNPs. Drude model was employed for dielectric function of Au, and a complex refractive index  $n_g = 2.4 + i \cdot 1$  was used for graphene [21]. The solid lines in Fig. 4 show the calculated  $Q$ -values as the function of wavelength for Au hemispheres on  $\text{SiO}_2$  without graphene and gap between the two Au hemispheres are 0.5 nm (circles), 1 nm (squares) and 3 nm (triangles), respectively. When the separation between the two Au particles is wide enough, the interference between them becomes weak and the wavelength of resonant absorption peak approaches that of a single Au particle. With the decrease of separation between the AuNPs, the field interference between them becomes stronger and introduces a red shift of the LSPR absorption wavelength, which agrees with our experimental results shown in Fig. 3 for larger AuNPs. The dashed lines in Fig. 4 show the calculated  $Q$ -values when a layer of graphene is placed on the substrate surface between Au hemisphere and  $\text{SiO}_2$  substrate. Evidently the conductivity of this graphene layer damps the plasmonic resonance, which results in a broadening and slightly red-shift of the LSPR absorption peaks. This agrees well with the measured transmittance shown in Fig. 3 and suggests the presence of

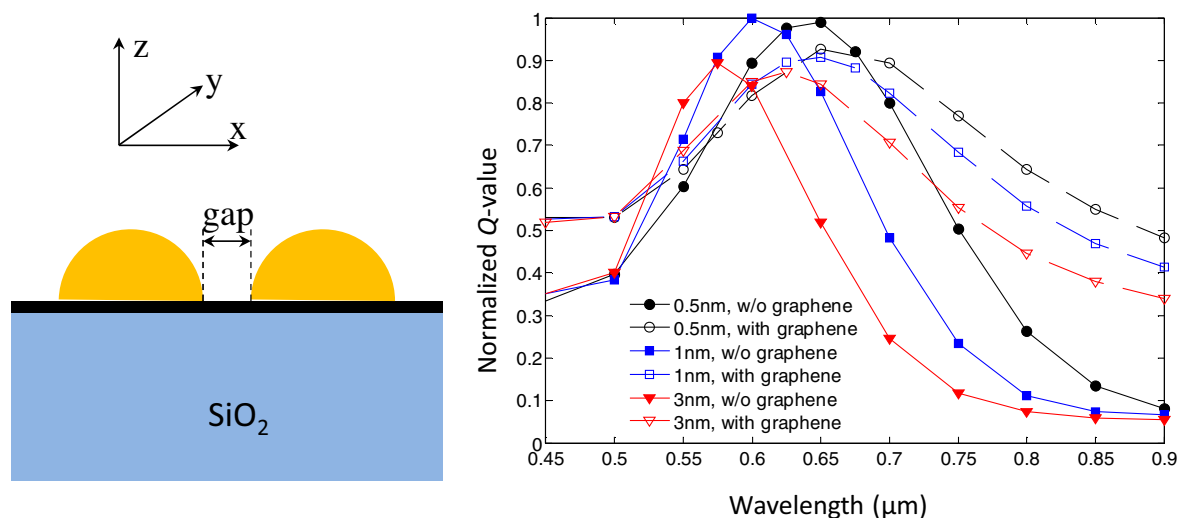


**Fig. 4 – Calculated  $Q$ -values of two Au nanoparticles on a  $\text{SiO}_2$  substrate without (solid lines) and with (dashed lines) a graphene layer on the interface. The gaps between the two Au hemispheres are 0.5 nm (circles), 1 nm (square) and 3 nm (triangles), separately. (A color version of this figure can be viewed online.)**

graphene causes minor degradation of the electromagnetic field on the SERS substrates.

The Raman spectra taken on the four AuNP/graphene samples shown in Fig. 2 are depicted in Fig. 5. The peaks are indexed as G, 2D and D peaks for graphene. For defect-free graphene there are two intrinsic peaks corresponding respectively to G band ( $1585\text{ cm}^{-1}$ , a primary first-order vibration mode as a result of the doubly degenerate zone center  $E_{2g}$  mode) and 2D band ( $2685\text{ cm}^{-1}$ , a second order scattering of zone-boundary phonons) [3,22]. The D peak ( $1345\text{ cm}^{-1}$ ) is also second order scattering process involving a defect site and a phonon, and it is usually used for defect diagnosis [3]. The intensity of original graphene spectrum is also included in Fig. 5 and multiplied by a factor of 10 to make a better comparison. While their positions are approximately the same, the G peak and 2D peak intensities of all samples with AuNPs shows a great enhancement by more than an order of magnitude as compared to original graphene's. This enhancement increases monotonically with the AuNP dimension and reaches the maximum of a factor of around 40 (2D peak) to 80 (G peak) at both nominal thicknesses of 8 and 12 nm, respectively, by comparing the peak intensity. The relative intensity of 2D over G peak ratio is obviously suppressed and even reversed with increasing nominal Au film thickness due to the different enhancement factors for 2D and G peaks, respectively. This enhancement is a result of charge doping from metallic NPs on graphene [3,23], which significantly affects the scattering intensity via electron–electron interaction [7]. The larger increase of D peak at greater nominal Au thickness is probably an indication of more defects generated at the AuNP/graphene interface during the Au growth at the elevated temperatures for longer time. Nevertheless, these results confirm the enhanced Raman spectroscopy of AuNP/graphene as a SERS substrate.

The SERS spectrum of R6G on a AuNP/graphene/SiO<sub>2</sub>/Si (R6G/AuNP/graphene/SiO<sub>2</sub>/Si) sample with 8 nm nominal Au

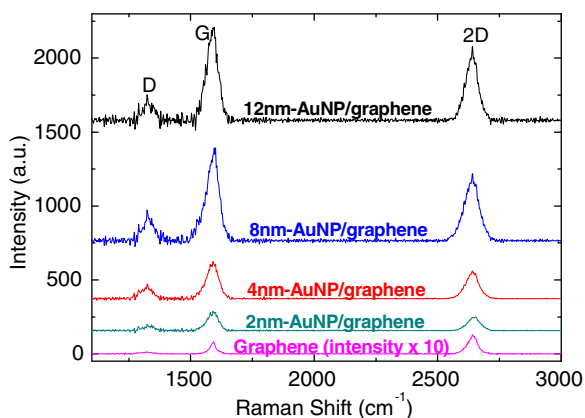


**Fig. 5 – Comparison of Raman spectra for samples with different nominal Au film thicknesses. The intensity of original graphene spectrum has been multiplied by a factor of 10 for better comparison. Curves have been shifted without changing the magnitudes, and baselines were removed for the comparison. (A color version of this figure can be viewed online.)**

is compared in Fig. 6 with those on three control samples of SiO<sub>2</sub>/Si (R6G/SiO<sub>2</sub>/Si), graphene/SiO<sub>2</sub>/Si (R6G/graphene/SiO<sub>2</sub>/Si) and AuNP/SiO<sub>2</sub>/Si (R6G/AuNP/SiO<sub>2</sub>/Si) after coating R6G dyes. The exciting laser power was kept at a low level of about 1 mW to avoid bleaching of the dyes. It was extremely difficult to obtain clear Raman spectrum for R6G/SiO<sub>2</sub>/Si, and the spectrum looks like a straight line (black). For R6G/graphene/SiO<sub>2</sub>/Si (blue), some of the R6G peaks can be observed with low intensity and the spectrum will be used as a reference for evaluating the SERS enhancement. Considerable enhancement on the R6G signature is obtained on SERS substrates with AuNPs, which is anticipated from the electromagnetic enhancement due to the LSPR on the AuNPs. By comparing the feature peak of R6G at  $1363\text{ cm}^{-1}$ , the enhancement by a factor of 21 can be estimated for R6G/AuNP/SiO<sub>2</sub>/Si with respect to the R6G/graphene/SiO<sub>2</sub>/Si reference sample by comparing the peak intensity. Interestingly, higher R6G sensitivity by further enhancement of approximately 400% (with a factor of 86 over the R6G/graphene/SiO<sub>2</sub>/Si reference sample) was observed on R6G/AuNP/graphene/SiO<sub>2</sub>/Si as compared to R6G/AuNP/SiO<sub>2</sub>/Si counterpart, suggesting graphene plays an important role in further improving the SERS sensitivity through interactions with plasmonic AuNPs. Note a comparable but slightly larger gap coverage of 49.7% is obtained on the AuNP/SiO<sub>2</sub>/Si substrate, in contrast to 45% in the AuNP/graphene/SiO<sub>2</sub>/Si (Table 1). The fact of much enhanced R6G SERS signature observed on the latter suggests the role of graphene is not simply limited to a geometric effect. In particular, these enhancement factors of 21–86 achieved in this work are remarkably greater than those of about 4.4–6.1, which are estimated by comparing the strongest peak at  $1363\text{ cm}^{-1}$  for CuPc, on AuNP SERS substrates fabricated on SiO<sub>2</sub>/Si and graphene using *ex situ* method [6]. It is also worth pointing out that the 400% improvement of AuNP/graphene/SiO<sub>2</sub>/Si over AuNP/SiO<sub>2</sub>/Si is about 3 times of that achieved on the *ex situ* fabricated substrates with a similar configuration.

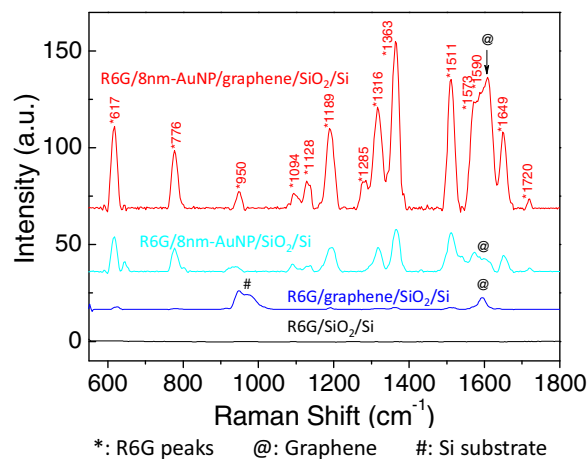


**Fig. 6 – Comparisons of Raman spectra for R6G on 8 nm-AuNP/graphene/SiO<sub>2</sub>/Si (red), 8 nm-AuNP/SiO<sub>2</sub>/Si (cyan), graphene/SiO<sub>2</sub>/Si (blue) and bare SiO<sub>2</sub>/Si (black). Curves have been shifted without changing the magnitudes, and baselines were removed for the comparison. (A color version of this figure can be viewed online.)**

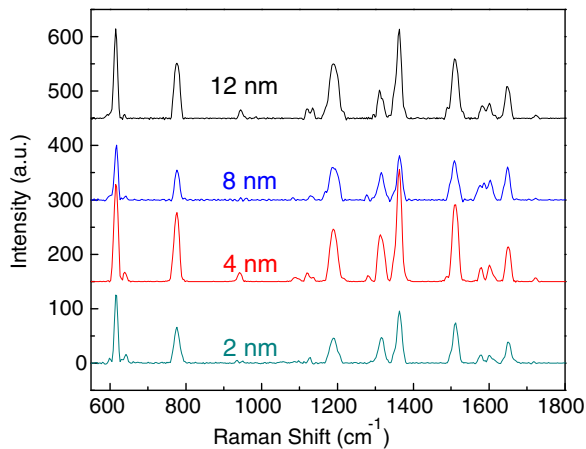


**Fig. 7 – Raman spectra of R6G/AuNP/graphene/SiO<sub>2</sub>/Si substrate with different nominal Au film thickness of 2 nm (dark cyan), 4 nm (red), 8 nm (blue) and 12 nm (black). The spectra were shifted for better display without changing the magnitudes, and baselines were removed for the comparison. (A color version of this figure can be viewed online.)**

The Raman spectra of R6G were taken using AuNP/graphene substrates with different nominal Au film thickness of 2, 4, 8, 12 nm and the results are compared in Fig. 7. Interestingly, the amplitudes of the R6G SERS peaks are more or less comparable on all samples while the highest was observed in 4 nm sample, which has the second largest inter-AuNP gap coverage area. Since a larger gap coverage occurs at a smaller AuNP dimension while no obvious trend could be observed in SERS signature strength of R6G, this result raises a question on the role of uncovered graphene surface in the gap in enhancing the R6G SERS sensitivity.

To shed some lights on the role of graphene in the enhanced SERS sensitivity of R6G on AuNP/graphene/SiO<sub>2</sub>/Si, we have simulated the two dimensional distribution of electrical field  $|E_x|$  on two different planes with respect to the AuNP/SiO<sub>2</sub> interface, and the stimulating source is a plane wave with a single polarized  $E_x$  component illuminated upward from the bottom. Fig. 8(a) and (b) show the field  $|E_x|$  distributions on the  $xz$ -plane at  $y = 0$ , while Fig. 8(c) and (d) show  $|E_x|$  distributions on the  $xy$ -plane at  $z = 0$ . Fig. 8(a) and (c) and (b and d) were obtained with and without graphene, respectively. The gap between the two Au hemispheres is 3 nm. In both cases, compared to everywhere else the magnitude of electrical field  $E_x$  is significantly higher at the edge of AuNPs, especially in the gap region between the AuNPs. However, the comparison between Fig. 8(a) and (c), and Fig. 8(b) and (d) indicates that the magnitude of electrical field in both planes is slightly reduced in the presence of the graphene layer. Fig. 9 plots the magnitude of electrical field  $E_x$  along the  $x$  axis ( $y = z = 0$ ) on the interface between AuNPs and SiO<sub>2</sub>, which illustrates that the electrical field is reduced considerably when the graphene layer is inserted between AuNPs and SiO<sub>2</sub>. This reduced electrical field is attributed to the conductivity of graphene which dissipates the near field on and around the AuNP/SiO<sub>2</sub> and thus causes damping of the plasmonic resonance. This microscopic effect is consistent with

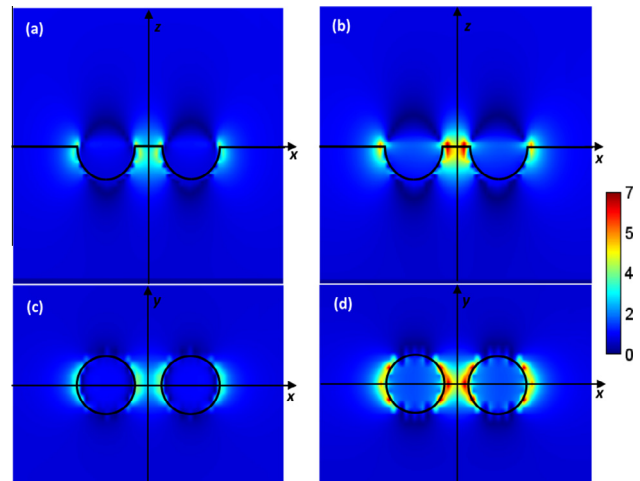


**Fig. 8 – Calculated two dimensional electrical field  $|E_x|$  distributions on the  $xz$ -plane at  $y = 0$  (a and b) and on the  $xy$ -plane at  $z = 0$  (c and d), for the Au/SiO<sub>2</sub> interface with (a and c) and without (b and d) a graphene layer. (A color version of this figure can be viewed online.)**

the reduced Q factor in macroscopic optical transmittance measurement discussed earlier in Figs. 3 and 4. Fig. 9 also indicates that the plasmonically enhanced near field only exists in the immediate proximity of the AuNP within about 1–2 nm damping distance. The interaction between AuNPs will not be significant when the gap width, which is in the range of 7–9 nm as shown in Table 1, is considerably larger than this damping distance. This means an optimal SERS substrate should have both large gap coverage area and the small gap width on the order of 2–4 nm to be covered fully with plasmonically enhanced near field. Further reduction of the inter-AuNP gap width will be important to further enhancing the SERS sensitivity.

Apparently, the significant amplitude increase of localized electromagnetic field around the plasmonic AuNPs plays a critical role in enhancing the R6G Raman signature on both

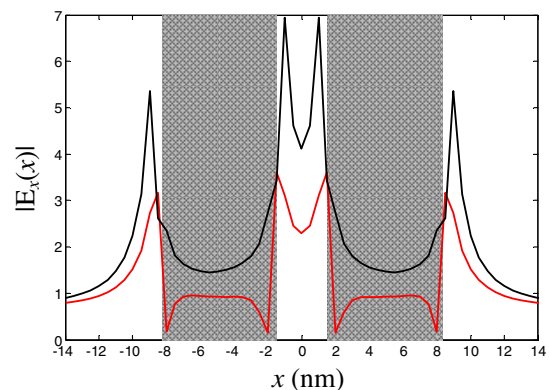


**Fig. 9 – Calculated electrical field along the  $x$ -axis ( $y = z = 0$ ) with (red) and without (black) the graphene layer on the Au/SiO<sub>2</sub> interface. Shaded areas indicate locations of Au particles. (A color version of this figure can be viewed online.)**

AuNP/SiO<sub>2</sub>/Si and AuNP/graphene/SiO<sub>2</sub>/Si substrates. However, it cannot be responsible for the further enhanced R6G SERS sensitivity observed in the latter based on Fig. 9. To gain some further insights on the role of graphene in the enhanced SERS sensitivity, we have made GFETs on SiO<sub>2</sub>/Si substrates with and without AuNPs. Fig. 10 compares four source-drain current  $I_{DS}$  as function of back gate voltage  $V_{BG}$  on a representative GFET before and after AuNPs of 8 nm nominal thickness were deposited on the GFET channel in air and in vacuum, respectively. The deposition of AuNPs shifts the Dirac point towards positive side as expected from the p-type doping of Au to graphene whether in vacuum or in air [24]. It should be noted that both p-type and n-type doping may be induced by deposition of metals depending on the work function alignment of the specific metal selected with respect to graphene's. For example, n-type doping is typically reported for graphene with plasmonic AgNPs [17]. In addition to the Dirac point shift, the doping also results in enhanced conductivity of graphene as illustrated from the Dirac point shift upwards after AuNP deposition in both cases of vacuum and in air (Fig. 10). Comparing the  $I_{DS}$ - $V_{BG}$  curves of in-vacuum and in-air cases, whether with or without AuNPs, a positive shift of the Dirac point from in-vacuum to in-air is clearly revealed. This amounts a large Dirac point shift up to +30 V from graphene only in vacuum to graphene with AuNPs in air. Based on this result, the AuNP/graphene is heavily p-doped in air due to the combined doping effect of AuNPs and molecules in air. This suggests the interface to the graphene is most probably negatively charged via exposure to air and deposition of AgNPs, which stabilizes holes in graphene and hence results in p-doping in graphene [25]. In particular, the doping caused by AuNPs will be non-uniform and will be stronger nearer the AuNPs where the plasmonic near field locates. On the other hand, the R6G molecules are positively charged in solution by losing the Cl<sup>-</sup> anions (Fig. 1) [26]. Based on this, we hypothesize the role of graphene in enhancing SERS sensitivity of R6G via chemical mechanism, which has

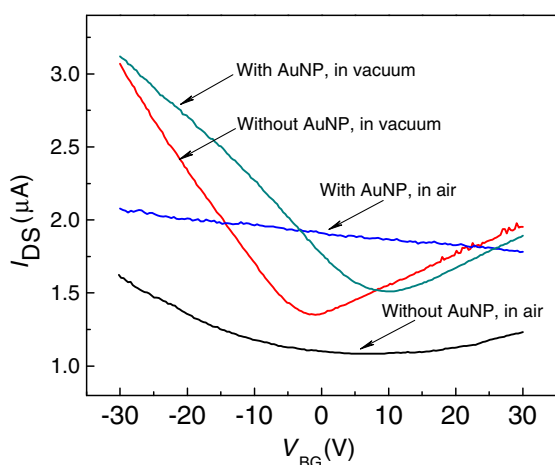


**Fig. 10** – Source-drain current  $I_{DS}$  vs. back gate voltage  $V_{BG}$  measured in air and vacuum, respectively, on a GFET device before and after AuNPs were deposited on the GFET channel. Source-drain voltage  $V_{DS} = 20$  mV for all measurements. (A color version of this figure can be viewed online.)

been recognized that the role of graphene on SERS enhancement is unlikely electromagnetic type, and chemical mechanisms play the dominant role instead, which may be classified into non-resonance molecular-to-substrate interaction and resonance charge-transfer or charge transfer [5,27,28]. In the absence of plasmonic nanoparticles, SERS signature of methylene blue on graphene substrates was found enhanced when graphene's Fermi level is tuned by electrical field or chemical doping and this enhancement was attributed to the possible nonresonance chemical interaction mechanism, while the microscopic mechanism remains unclear [28]. Compared to the case of AuNP/substrate SERS, where electromagnetic mechanism obviously dominates the enhancement, the further enhancements observed in our *in situ* fabricated AuNP/graphene SERS substrate may be attributed to a similar mechanism of non-resonance chemical interaction, while the involvement of plasmonic resonance to further enhance such a chemical effect cannot not be ruled out at this point. Further investigation is certainly important to understand the microscopic mechanism of graphene in enhanced SERS. In addition, the negatively charged interface near graphene may facilitate R6G molecules adsorption to graphene especially in the area surrounding the AuNPs. This argument is supported by the observation of no clear trend in R6G Raman signature sensitivity when the inter-AuNP gap coverage area varies systematically as shown in Fig. 7, since it is the area immediately surrounding the AuNPs that benefits from the plasmonically enhanced electromagnetic field for higher SERS sensitivity. This result therefore suggests a higher SERS sensitivity may be achieved but further optimization of the inter-AuNP gap width on top of the large gap coverage area reported in this work.

#### 4. Conclusion

In conclusion, an *in situ* process has been developed for controllable self-assembly of AuNPs on CVD graphene with large inter-AuNP gap coverage area up to 69.6% between the AuNPs. R6G molecule SERS were investigated as an illustration on this hybrid AuNP/graphene/SiO<sub>2</sub>/Si substrate. This AuNP/graphene nanohybrid provides a high-sensitivity SERS substrate due to both enhanced optical electromagnetic field in the gap that resulted from the LSPR effect of AuNPs and the strongly p-doped graphene that further promoted interaction between R6G molecule and substrate. R6G SERS enhancements, by a factor of 21 and 86, as compared to graphene/SiO<sub>2</sub>/Si substrate have been obtained on AuNP/SiO<sub>2</sub>/Si and AuNP/graphene/SiO<sub>2</sub>/Si substrates, separately, and are considerably greater than the previous reported enhancements on *ex situ* fabricate SERS substrates. The further enhancement by 400% with implementation of graphene on the AuNP/SiO<sub>2</sub>/Si substrate can be attributed to the chemical mechanism through p-doped graphene, which enhances R6G adsorption and non-resonance molecule-substrate interaction. Our results suggest AuNP/graphene nanohybrid is a promising SERS substrate for high sensitivity molecule detection and an optimal SERS substrate should have both large gap coverage area and the small gap width that is covered with plasmonically enhanced near field.

## Acknowledgments

The authors acknowledge support in part by U.S. Army Research Office (ARO) contract No. ARO-W911NF-12-1-0412, and U.S. National Science Foundation (NSF) contracts Nos. NSF-DMR-1105986 and NSF EPSCoR-0903806, and matching support from the State of Kansas through Kansas Technology Enterprise Corporation. J.W. thanks Professor Cindy L. Berrie for helpful discussions on R6G.

## REFERENCES

- [1] Freudiger CW, Min W, Saar BG, Lu S, Holtom GR, He CW, et al. Label-free biomedical imaging with high sensitivity by stimulated Raman scattering microscopy. *Science* 2008;322(5909):1857–61.
- [2] Fleischmann M, Hendra PJ, McQuillan AJ. Raman-spectra of pyridine adsorbed at a silver electrode. *Chem Phys Lett* 1974;26(2):163–6.
- [3] Xu WG, Mao NN, Zhang J. Graphene: a platform for surface-enhanced Raman spectroscopy. *Small* 2013;9(8):1206–24.
- [4] Ling X, Xie LM, Fang Y, Xu H, Zhang HL, Kong J, et al. Can graphene be used as a substrate for Raman enhancement? *Nano Lett* 2010;10(2):553–61.
- [5] Xie LM, Ling X, Fang Y, Zhang J, Liu ZF. Graphene as a substrate to suppress fluorescence in resonance Raman spectroscopy. *J Am Chem Soc* 2009;131(29):9890–1.
- [6] Xu WG, Ling X, Xiao JQ, Dresselhaus MS, Kong J, Xu HX, et al. Surface enhanced Raman spectroscopy on a flat graphene surface. *Proc Natl Acad Sci U S A* 2012;109(24):9281–6. Taking the pristine CuPc/SiO<sub>2</sub>/Si as reference, SERS enhancements were evaluated in the literature by comparing the Raman spectra of CuPc dye molecules coated on different substrates: a factor of 14 for graphene/CuPc/SiO<sub>2</sub>/Si, 61 for Au/CuPc/SiO<sub>2</sub>/Si and 85 for Au/graphene/CuPc/SiO<sub>2</sub>/Si. To make reasonable comparisons, the enhancement factors as compared to graphene/CuPc/SiO<sub>2</sub>/Si can be calculated as: 61/14 = 4.4 for Au/CuPc/SiO<sub>2</sub>/Si and 85/14 = 6.1 for Au/graphene/CuPc/SiO<sub>2</sub>/Si. The SERS was further enhanced by a factor of 140% for Au/graphene/CuPc/SiO<sub>2</sub>/Si as compared to Au/CuPc/SiO<sub>2</sub>/Si.
- [7] Schedin F, Lidorikis E, Lombardo A, Kravets VG, Geim AK, Grigorenko AN, et al. Surface-enhanced Raman spectroscopy of graphene. *ACS Nano* 2010;4(10):5617–26.
- [8] Atwater HA, Polman A. Plasmonics for improved photovoltaic devices. *Nat Mater* 2010;9(3):205–13.
- [9] He S, Liu K-K, Su S, Yan J, Mao X, Wang D, et al. Graphene-based high-efficiency surface-enhanced Raman scattering-active platform for sensitive and multiplex DNA detection. *Anal Chem* 2012;84:4622–7.
- [10] Lv R, Li Q, Botello-Mendez AR, Hayashi T, Wang B, Berkdemir A, et al. Nitrogen-doped graphene: beyond single substitution and enhanced molecular sensing. *Sci Rep* 2012;2:586.
- [11] Liu JW, Xu GW, Rochford C, Lu RT, Wu J, Edwards CM, et al. Doped graphene nanohole arrays for flexible transparent conductors. *Appl Phys Lett* 2011;99(2):023111.
- [12] Xu GW, Liu JW, Wang Q, Hui RQ, Chen ZJ, Maroni VA, et al. Plasmonic graphene transparent conductors. *Adv Mater* 2012;24(10):OP71–6.
- [13] Gaspar D, Pimentel AC, Mateus T, Leitao JP, Soares J, Falcao BP, et al. Influence of the layer thickness in plasmonic gold nanoparticles produced by thermal evaporation. *Sci Rep* 2013;3:1469.
- [14] Li ZZ, Baca J, Wu J. In situ switch of boron nanowire growth mode from vapor–liquid–solid to oxide-assisted growth. *Appl Phys Lett* 2008;92(11):113104.
- [15] Wang FL, Wang Q, Xu GW, Hui RQ, Wu J. Light trapping on plasmonic–photonic nanostructured fluorine-doped tin oxide. *J Phys Chem C* 2013;117(22):11725–30.
- [16] Available from <http://imagej.nih.gov/ij/>.
- [17] Xu G, Lu R, Liu J, Chiu H-Y, Hui R, Wu J. Photodetection based on ionic liquid gated plasmonic Ag nanoparticle/graphene nanohybrid field effect transistors. *Adv Opt Mater* 2014;2(8):729–36.
- [18] Yun SH, Wu JZ, Dibos A, Gao X, Karlsson UO. Growth of inclined boron nanowire bundle arrays in an oxide-assisted vapor–liquid–solid process. *Appl Phys Lett* 2005;87(11):113109.
- [19] Yun SH, Wu JI, Dibos A, Zou XD, Karlsson UO. Self-assembled boron nanowire Y-junctions. *Nano Lett* 2006;6(3):385–9.
- [20] FullWAVE simulation package version 60. R-Soft Design Group; 2007.
- [21] Wang XF, Chen YP, Nolte DD. Strong anomalous optical dispersion of graphene: complex refractive index measured by Picometrology. *Opt Express* 2008;16(26):22105–12.
- [22] Ferrari AC, Meyer JC, Scardaci V, Casiraghi C, Lazzeri M, Mauri F, et al. Raman spectrum of graphene and graphene layers. *Phys Rev Lett* 2006;97(18):187401.
- [23] Das A, Pisana S, Chakraborty B, Piscanec S, Saha SK, Waghmare UV, et al. Monitoring dopants by Raman scattering in an electrochemically top-gated graphene transistor. *Nat Nanotechnol* 2008;3(4):210–5.
- [24] Lee EJJ, Balasubramanian K, Weitz RT, Burghard M, Kern K. Contact and edge effects in graphene devices. *Nat Nanotechnol* 2008;3(8):486–90.
- [25] Baeumer C, Rogers SP, Xu R, Martin LW, Shim M. Tunable carrier type and density in graphene/PbZr<sub>0.2</sub>Ti<sub>0.8</sub>O<sub>3</sub> hybrid structures through ferroelectric switching. *Nano Lett* 2013;13(4):1693–8.
- [26] Milanova D, Chambers RD, Bahga SS, Santiago JG. Electrophoretic mobility measurements of fluorescent dyes using on-chip capillary electrophoresis. *Electrophoresis* 2011;32:3286–94.
- [27] Jensen L, Aikens CM, Schatz GC. Electronic structure methods for studying surface-enhanced Raman scattering. *Chem Soc Rev* 2008;37:1061–73.
- [28] Hao QZ, Morton SM, Wang B, Zhao YH, Jensen L, Huang TJ. Tuning surface-enhanced Raman scattering from graphene substrates using the electric field effect and chemical doping. *Appl Phys Lett* 2013;102(1):011102.